AD-A172 566 TEMPERATURE DEPENDENCE ON THE LOW AND HIGH FREQUENCY RAMAN SCATTERING PRO..(U) HOWARD UNIV WASHINGTON DC LASER CHEMISTRY DIV G E WALRAFEN ET AL. OCT 86 1/1

UNCLASSIFIED TR-23-ONR N00014-80-C-0305 F/G 7/4 NL

[redacted]

END

DATE FILMED

11-86

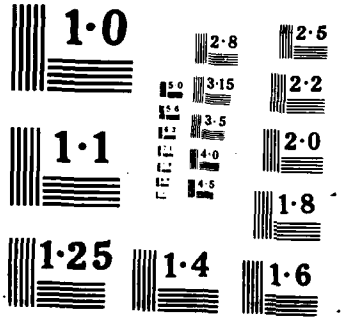
1·0
2·8
2·5
3·15
2·2
3·5
1·1
2·0
4·0
4·5
1·8
1·25
1·4
1·6

Unclassified

SECURITY CLASSIFICATION OF THIS PAGE

(2)

REPORT D

DTIC ELECTE S OCT 07 1986 D

AD-A172 566

1a. REPORT SECURITY CLASSIFICATION Unclassified	
2a. SECURITY CLASSIFICATION AUTHORITY	3. DISTRIBUTION/AVAILABILITY OF REPORT
2b. DECLASSIFICATION / DOWNGRADING SCHEDULE	Unlimited, unrestricted
4. PERFORMING ORGANIZATION REPORT NUMBER(S) ~~ONR~~-TR-23-ONR	5. MONITORING ORGANIZATION REPORT NUMBER(S)
6a. NAME OF PERFORMING ORGANIZATION Laser Chemistry Division Chemistry/howard Univ.	6b. OFFICE SYMBOL (If applicable)
6c. ADDRESS (City, State, and ZIP Code) 500 College Street Washington, DC 20059	7a. NAME OF MONITORING ORGANIZATION Office of Naval Research Chemistry Division
	7b. ADDRESS (City, State, and ZIP Code) Arlington, VA 22217-5000
8a. NAME OF FUNDING / SPONSORING ORGANIZATION	8b. OFFICE SYMBOL (If applicable)
	9. PROCUREMENT INSTRUMENT IDENTIFICATION NUMBER N00014-80-C-0305
8c. ADDRESS (City, State, and ZIP Code)	10. SOURCE OF FUNDING NUMBERS

PROGRAM ELEMENT NO	PROJECT NO	TASK NO	WORK UNIT ACCESSION NO

11. TITLE (Include Security Classification)

Temperature dependence of the low and high frequency Raman scattering from liquid water

12. PERSONAL AUTHOR(S)

Walrafen, G. E., Fisher, M.R., Hokmabadi, M.S., Yang, W. H.

13a. TYPE OF REPORT	13b. TIME COVERED	14. DATE OF REPORT (Year, Month, Day)	15. PAGE COUNT
Technical	FROM 4/85 TO 10/86		16

16. SUPPLEMENTARY NOTATION

17. COSATI CODES		
FIELD	GROUP	SUB-GROUP

18. SUBJECT TERMS (Continue on reverse if necessary and identify by block number)

Water, Raman scattering, temperature dependence

19. ABSTRACT (Continue on reverse if necessary and identify by block number)

Bose-Einstein corrected Raman spectra of water were measured between 3.5 and 89.3 °C. The low frequency Raman spectra lead to a value of 2.6 ± 0.1 kcal/mole for the rupture of the hydrogen bonds. It is in good agreement with measurements obtained by other techniques.

Absolute Raman spectra in the OH stretching region yield a precise isosbestic point at 3425 cm^{-1}. This is indicative of an equilibrium between hydrogen bonding and non-hydrogen bonding classes of interaction. Difference spectra in this region establish the presence of the equilibrium and indicate that the OH oscillator strength is conserved in terms of the two classes of bonding.

DTIC FILE COPY

86 10 7 002

20. DISTRIBUTION / AVAILABILITY OF ABSTRACT ☒ UNCLASSIFIED/UNLIMITED ☐ SAME AS RPT ☐ DTIC USERS	21. ABSTRACT SECURITY CLASSIFICATION UNCLASSIFIED
22a. NAME OF RESPONSIBLE INDIVIDUAL Walrafen, G.E.	22b. TELEPHONE (Include Area Code) 202-636-6897
	22c. OFFICE SYMBOL

DD FORM 1473, 84 MAR

83 APR edition may be used until exhausted

All other editions are obsolete

SECURITY CLASSIFICATION OF THIS PAGE

UNCLASSIFIED

OFFICE OF NAVAL RESEARCH

Contract N00014-80-C-0305

R & T Code 4131023

TECHNICAL REPORT NO. 23

Temperature Dependence of the Low and High Frequency Raman Scattering from Liquid Water

by

G. E. Walrafen, M. R. Fisher, M. S. Hokamabadi, and W. H.-Yang

to be published in the Journal of Chemical Physics

Department of Chemistry
Howard University
Washington, DC 20059

028622JCP
Running Title: Raman scattering from liquid water

Temperature dependence of the low- and high-frequency Raman scattering from liquid water

G. E. Walrafen, M. R. Fisher,[a] M. S. Hokmabadi, and W.-H. Yang[b]
Chemistry Department, Howard University, Washington, D.C. 20059

(Recieved 23 December 1985; accepted 31 July 1986)

Low frequency $\Delta\tilde{\nu} = 0$–$350\ cm^{-1}$, Raman intensity data were obtained from liquid water between 3.5 and 89.3 °C using holographic grating double and triple monochromators. The spectra were Bose–Einstein (BE) corrected, $I/(1+n)$, and the total integrated (absolute) contour intensities were treated by an elaboration of the Young–Westerdahl (YW) thermodynamic model, assuming conservation of hydrogen-bonded (HB) and nonhydrogen-bonded (NHB = bent and/or stretched, O–H O) nearest-neighbor O–O pairs. A ΔH°_1 value of 2.6 ± 0.1 kcal/mol O–H ··· O or 5.2 ± 0.2 kcal/mol H_2O (11 kJ/mol O–H ··· O, or 22 kJ/mol H_2O) resulted for the HB→NHB process. This intermolecular value agrees quantitatively with Raman and infrared ΔH° values from one- and two-phonon OH-stretching regions, and from molecular dynamics, depolarized light scattering, neutron scattering, and ultrasonic absorption, thus indicating a common process. A population involving partial covalency of, i.e., charge transfer into, the H ··· O units of linear and/or weakly bent hydrogen bonds, O–H ··· O; is transformed into a second high energy population involving bent, e.g., 150° or less, and/or stretched, e.g., 3.2 Å, but otherwise strongly cohesive O–H O interactions. All difference spectra from the fundamental OH-stretching contours cross at the $X(Z,X+Z)Y$ isobestic frequency of 3425 cm^{-1}. Also, total integrated Raman intensity decreases occurring below 3425 cm^{-1} with temperature rise were found to be proportional to the total integrated intensity increases above 3425 cm^{-1}, indicating conservation among the HB and NHB OH-stretching classes. From the enthalpy of vaporization of water at 0 °C, and the ΔH°_1 of 2.6 kcal/mol O–H ··· O, the additional enthalpy, ΔH°_2, needed for the complete separation of the NHB O–O nearest neighbors is ~3.2 kcal/mol O–H ··· O or ~6.4 kcal/mol H_2O (13 kJ/mol O–H ··· O or 26 kJ/mol H_2O). The NHB O–O nearest neighbors are held by forces other than those involving H ··· O partial covalency, i.e., electrostatic (multipole), induction, and dispersion forces. The NHB O–O pairs do not appear to produce significant intermolecular Raman intensity because they lack H ···O bond polarizability, but the corresponding NHB OH oscillators do contribute weakened Raman intensity above 3425 cm^{-1}. An ideal solution thermodynamic treatment employing $\Delta H^{\circ}_1 = 2.6$ kcal/mol O–H ··· O, the HB mole fraction, and the vapor heat capacity, yielded a very satisfactory specific heat value of 1.1 cal deg^{-1} g^{-1} H_2O at 0 °C. The NHB mole fraction, f_u, from the YW treatment is negligibly small, 0.06 or less, for $t < -50$ °C. However, f_u increases to 0.16 at 0 °C, and $f_u \approx 1$ at 1437 °C, where recent shock-wave Raman measurements indicate loss of all partially covalent, charge transfer hydrogen bonding.

I. INTRODUCTION

The low-frequency Raman spectrum from liquid water, $\Delta\tilde{\nu} = 0$–$350\ cm^{-1}$, is composed of (at least) two, weak, broad features at nominal positions of 170 and 60 cm^{-1}. The 170 cm^{-1} band was discovered by Segrè in 1931[1] and the weaker 60 cm^{-1} band by Bolla in 1932.[2] Microdensitometer tracings presented by Segrè clearly indicate that both the 170 cm^{-1} intensity, and the Raman intensity near 3250 cm^{-1} in the OH-stretching region, decrease relative to other Raman bands with temperature rise. Such results were interpreted by Segre as a breakdown of intermolecular structure, and agree with data of this work.

Similar temperature effects were observed by Bolla for the 60 cm^{-1} band, as well as for the Raman intermolecular librational and OH-stretching bands.[2] Because of the high quality of Bolla's low-frequency spectra, correction for the Bose–Einstein (BE) thermal population factor and stray-light background was accomplished recently.[3] These corrections yielded agreement with modern results.

The 170 cm^{-1} Raman band arises from the vibration of an oxygen atom against its nearest-neighbor oxygen when a linear or at most weakly bent hydrogen bond, O–H ··· O, is present between them. This motion is often described alternatively as a restricted translation, but one that is perpendicular to the hydrogen-bond O–H ··· O direction, i.e., as a bending of the hydrogen bond.

Raman activity at 170 and 60 cm^{-1} occurs because of the partial covalency of,[4] or the charge transfer into,[5] the H ··· O part of the O–H ··· O unit. Without this partially co-

[a] Present address: Department of Chemistry, University of California, Irvine, CA 92717
[b] Permanent address: Institute of Physics, Chinese Academy of Science, Beijing, China

valent character, no change of the H ··· O bond polarizability could occur during vibration.

Quantum mechanical calculations, however, indicate that the partially covalent character of the hydrogen bond decreases with decrease of the O–H ··· O angle (below 180°).[6] This suggests[7] that the Raman polarizability derivative is a function of, and decreases very sharply for, O–H ··· O angles below some cut-off value, e.g., roughly 150°, see subsequent discussion.

In this work linear or weakly bent hydrogen bonds are designated by O–H ··· O, or by HB (hydrogen bonded). Strongly bent and/or stretched (ruptured) interactions are designated as nonhydrogen-bonded, NHB, or by O–H O, *without* dots. (The absence of dots indicates lack of partial covalency or charge transfer).

Numerous authors have now reported Raman and infrared results for the low-frequency region of water.[8–26] Moreover, a recent trend has been to report frequency reduced spectra $\omega I/(1+n)$, where $(1+n)$ is the one-phonon Bose–Einstein (BE) factor with $n = 1/(e^{\hbar\omega/kT} - 1)$, ω is the frequency, and I the Raman amplitude at ω[27–29]; or, temperature reduced spectra $I/(1+n)$, where only the BE correction has been made.[3] These reduced spectra involve different functionalities of the frequency dependent Raman coupling coefficient $c(\omega)$,[27–29] but in many cases no clear basis for the assumed functionality exists, because neutron inelastic scattering spectra are required to determine $c(\omega)$, and such spectra are often unavailable. However, a safe approach, employed here, is to ignore the Shuker–Gammon formalism entirely,[27] and simply to apply the BE correction, as clearly indicated by Placzek in 1934.[30] In any case, it should be made clear that either the $\omega I/(1+n)$ or the $I/(1+n)$ representation is, in principle, equivalent, with regard to any additional temperature dependence that remains after correction. The ω term is simply a temperature-independent multiplier, and therefore it cannot affect the corrected temperature dependence. On the other hand, failure to apply any temperature correction whatsoever causes the low-frequency Raman intensities from water to appear to decrease too rapidly with temperature rise.[12]

In previous (1966) low-frequency work involving water, a $\Delta H°$ value of about 5.6 kcal/mol was obtained from the temperature dependence of the Raman intensity.[12] BE correction was attempted, but it was inadequate, and the resulting $\Delta H°$ value was too large, as seen from the calculated heat capacity. However, with modern methods of data acquisition and computerized scanning and processing, it is easy to obtain BE corrected spectra, thus greatly reducing the labor involved when many corrected spectra at a series of temperatures are required. Moreover, BE reduction of the *total* scattering amplitude leads to a surprisingly simple and accurate base line not recognized previously[12] in which a strongly curving uncorrected base line was used. (Furthermore, no simple method of obtaining the base line for frequency reduced spectra was found here.) Thus, although the uncorrected Raman spectra obtained now and previously[12] do not differ substantially, the present BE correction yields accurate results which constitute the principal subject of this new work.

Another aspect of the present work involves difference Raman spectra obtained from the fundamental (one-phonon) intramolecular OH-stretching region, as well as the isosbestic frequency from the $X(Z,X+Z)Y$ spectra. Precise isosbestic points were also measured for the $X(ZZ)Y$, $X(Y,X+Z)Y$ and $X(ZX)Y$ orientations. In addition, precise isosbestic points were observed for $I(\mathrm{VV}) - 4/3I(\mathrm{VH})$, i.e., for α^2, but only the $X(Z,X+Z)Y$ data are presented here. The difference method yields results which are entirely consistent with previous Gaussian computer decompositions of the OH-stretching contours,[12,13,17,19,31] but it does not require assumptions related to component shapes or to the number of components.

The qualitative OH-stretching, OH-difference, and low-frequency Raman data are now presented.

II. EXPERIMENTAL PROCEDURES

Low-frequency Raman spectra were obtained with a J.Y. T800 triple monochromator, and with a J.Y. HG2S holographic grating double monochromator. The T800 is a holographic grating instrument of 800 mm focal length. It employes plane gratings in each of the three Czerny–Turner type monochromators in series. With the T800, data collection and processing was accomplished using a pulse discriminator, a custom interface, a Commodore 64 computer plus 1541 disk drive, and a HP 7470 plotter. The J.Y. HG2S system employed an EG&G model 1182 preamplifier discriminator, an ISA Spectra link photon counter, an ISA Columbia Data Products computer, and the HP 7470 plotter, although dc detection was also accomplished with a Keithly 414S picoammeter. BE corrected spectra $I/(1+n)$ and frequency reduced spectra $\omega I/(1+n)$ were obtained with the computers described.

Raman spectra were obtained in the low-frequency and OH-stretching regions under rigorously constant conditions of excitation intensity and detection geometry. These spectra were thus *absolute*, except that they were not calibrated in terms of $\mathrm{cm}^2\ \mathrm{mol}^{-1}\ \mathrm{sr}^{-1}$ vs temperature. This intensity constancy was verified by a series of scanning cycles in which the peak amplitude, e.g., of the OH-stretching peak, was determined to be the same within 3%, or less, when the water was returned to the same temperature after a long time interval. This procedure, which monitors long term drift, was used previously, where Raman OH-stretching overtone intensities were held constant to within 3% over periods of 10 h.[31]

A special Raman cell was used for measurement of the isosbestic frequency in the OH-stretching region. This cell was surrounded by an outer container having two open laser-beam ports (3 mm diameter) and one large, 10 × 10 cm, glass viewing window. The outer container was flushed with dry Ar to prevent condensation of moisture on the windows of the Raman cell. The Raman cell employed three windows, two in-line windows for laser excitation, and a third large (2 cm diameter) viewing window exactly at 90° to the other two. The in-line windows were exactly parallel to each other because they rested directly on precisely machined, parallel, stainless steel faces of the Raman cell.

The laser-beam position in the filled Raman cell was

held *precisely* fixed for the duration of a series of measurements. Invariance of the laser-beam position in the water is extremely important for quantitative intensity measurements under conditions of changing temperature. This invariance was accomplished by observing Newton's rings due to the backward laser reflection from the entrance (side) window. (Newton's rings were observed around a pinhole in a black card placed 3 m from the side window.) No cell adjustment whatsoever was required, or made, during the measurements. Moreover, when Newton's rings were invariant, the laser spot on the wall 3 m from the exit window was exactly fixed. If the laser-beam position in the filled Raman cell is not exactly perpendicular to the entrance (side) window of the cell, bending of the beam will occur as the refractive index of the water changes with temperature, and large intensity errors will result. Such errors can completely preclude the observation of precise isosbestic points, and may have contributed to an erroneous conclusion about the absence of the α^2 isosbestic point for water.[32] The temperature was maintained to ± 0.1 °C by pumping water or cold brine from an external themostated bath through the large rear chamber of the cell. However, the temperature of the sample water was measured accurately by placing the tip of a thermocouple 1 mm above the laser beam.

The water employed was distilled three times in a fused quartz still. This triple distilled water was found to be free of particulates, and to have an extremely low fluorescence level.[31]

A du Pont 310 analog computer was used for Gaussian analysis of low-frequency Raman contours.

III. EXPERIMENTAL RESULTS, DISCUSSION, AND INTERPRETATION

A. Low-frequency Raman data

Temperature reduced or BE corrected Raman spectra from water, $I/(1+n)$, obtained from $\sim$0–500 cm^{-1} under rigorously constant conditions of excitation and detection, i.e., absolute in the sense described in Sec. II, are shown in Fig. 1. Intensity maxima near 53 and 175 cm^{-1}, i.e., the nominal 60 and 170 cm^{-1} features, are obvious in the spectrum corresponding to 3.5 °C, top spectrum. A marked decline in the intensity of the 170 cm^{-1} feature is also evident with temperature rise to 89.3 °C, bottom spectrum.

Figure 1 shows four spectra in the temperature range from 3.5 to 89.3 °C in which a total of 12 quantitative temperature-reduced spectra were obtained. A single *constant* average base line was determined from examination of these 12 spectra, and tested as described next, see the curved lower lines in Fig. 1. This constant base line was drawn under all of the spectra by identical positioning of a metal template, shaped specifically to reproduce the average baseline exactly. The area above this base line from 0 to $\sim$325 cm^{-1} constitutes the total integrated contour intensity, whose temperature dependence refers to the HB→NHB transformation in water.

The base line shown in Fig. 1 arises from the stray-light level of the T800 triple monochromator. This base line was determined and tested by comparisons between the low-frequency BE corrected Raman spectra from water and from 96 wt. % H_2SO_4, both at 22 °C, and under the same excitation and detection conditions. The base line was tested further by obtaining low-frequency BE corrected Raman spectra from water using the HG2S double monochromator.

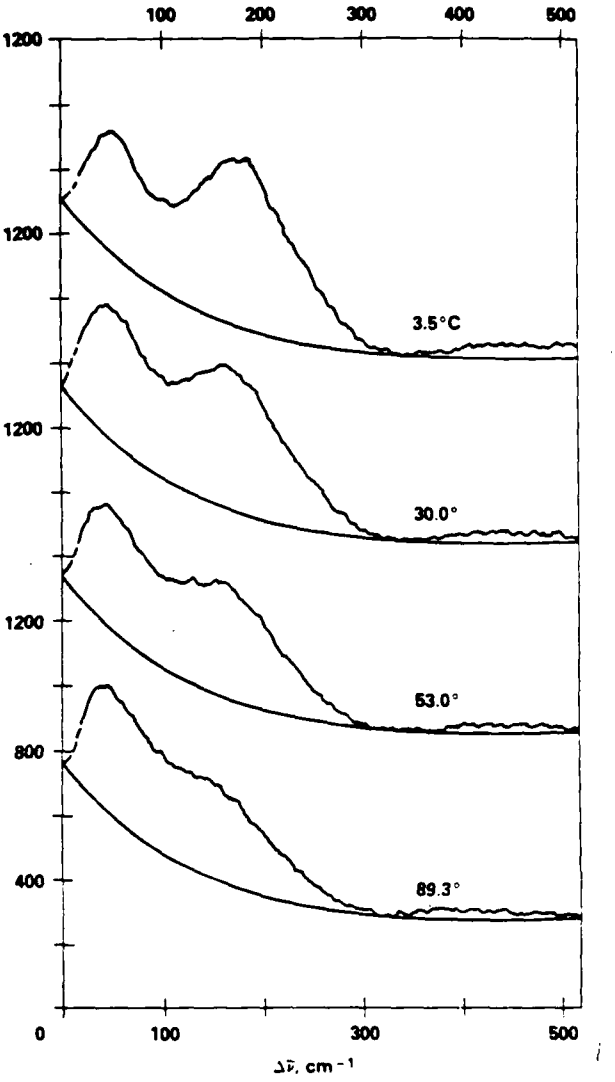

FIG 1 Bose-Einstein corrected low-frequency Raman (absolute) $X(Z,Z+X)Y$ spectra from water between 3.5 and 89.3 °C under rigorously constant conditions of excitation intensity and detection geometry. Note that because of superposition, the photon counts per second are not expressed at 800 c/s for the top three spectra.

The low-frequency BE corrected Raman spectrum from 96% H_2SO_4 displays, (1) a pronounced asymmetric feature peaking sharply at 25 cm^{-1} and showing a long region of downward concavity extending to 150 cm^{-1}, (2) a very weak (compared to water), broad O–H ··· O stretching contour centered near 155 ± 5 cm^{-1}, (3) an inflection at 115 cm^{-1} between the 25 and 155 cm^{-1} peaks, and (4) an intensity minimum at 280 cm^{-1}. All of these features occur below the H_2SO_4 and HSO_4^- deformation frequencies of 395 and 419 cm^{-1} (unresolved). The sharply peaking nature of the 25 cm^{-1} feature allowed the total scattering amplitude near $\Delta\bar{\nu} = 0$ cm^{-1} to be determined. The total scattering ampli-

TABLE I. Bose–Einstein corrected low-frequency total integrated contour intensities, I, for water at various temperatures, t °C.

t, °C	I
3.5	21.46
11.2	23.51
16.7	23.68
22.2	22.17
30.0	22.35
34.3	22.23
46.4	17.61
53.0	19.32
61.8	18.99
69.5	19.91
78.3	16.99
89.3	18.16

tude at 280 cm^{-1} could be measured directly. Further, the base line at the 115 cm^{-1} inflection could be estimated because of the shape and weakness of the neighboring 155 ± 5 cm^{-1} O–H ··· O feature. The entire base line from 96% H_2SO_4 was thus determined as a smooth curve having the same shape and upward concavity as that shown in Fig. 1. Furthermore, the relative amplitude of the 96% H_2SO_4 base line was found to match that obtained for water at 22 °C to within ± 5% over the entire range 0–300 cm^{-1}.

The base line slope of Fig. 1 was also tested with the HG2S double monochromator. For water, the same shape and upward concavity was observed with both of the HG2S and T800 instruments. The ratio of the total scattering amplitude near $\Delta\tilde{\nu} = 0$ to that at $\Delta\tilde{\nu} = 330$ cm^{-1} for the HG2S was only 13% larger than the corresponding ratio from the T800. This value is just outside the experimental uncertainty of ± 5% in the base line determination using the 96% H_2SO_4 comparison, and it indicates that the stray-light level of the T800 is slightly better than that of the HG2S, as noted previously.[3]

The total integrated BE corrected Raman intensities, $I/(1+n)$, i.e., the areas above the base lines in the region 0–325 cm^{-1} for all 12 quantitative spectra, are listed in Table I. These intensity data are plotted vs temperature in °C in Fig. 2, where the linear least squares fit of the data is shown by a dashed line. The linear least squares equation, not shown in the figure, is $I = 22.636 - 0.070\,847\ t$. The linear least squares slope of −0.0708 47 represents the *sole* significant feature of the data. This slope is required to obtain parameters relevant to the YW thermodynamic method,[33] discussed subsequently.

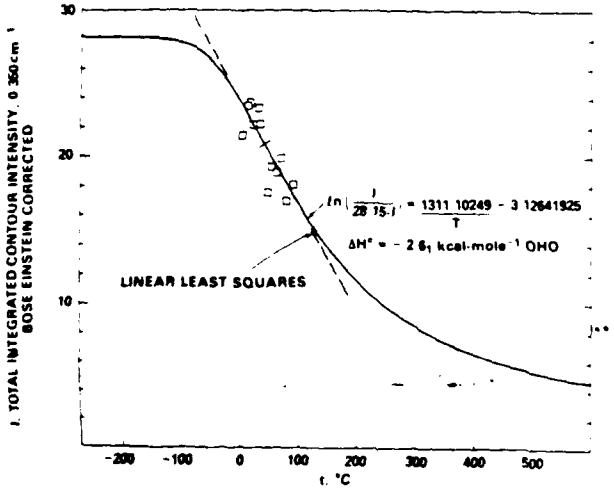

FIG. 2. Integrated Bose–Einstein corrected Raman intensities (□) from water vs temperature in °C.

B. Thermodynamic analysis

1. Determination of ΔH° for the HB→NHB transformation

Consider the unbonded to bonded transformation U→B, i.e., NHB→HB, between O–O nearest-neighbors in liquid water, where U refers to NHB O–O nearest neighbors, e.g., severely bent and/or stretched O–H O interactions; and B refers to partially covalent, linear and/or weakly bent, hydrogen bonds, O–H ··· O, that contribute to the low-frequency, 0–350 cm^{-1}, Raman intensity from water. The corresponding equilibrium constant is [B]/[U]. However, because of conservation of all O–O nearest neighbor concentrations, [U] + [B] = α, where α is constant.[34] The total integrated Raman intensity after Bose–Einstein correction, I, is considered to be proportional to the B concentration, $I = \beta$[B]. U is thought not to produce any intermolecular Raman contribution whatsoever. Substitution of $\alpha - I/\beta$ for [U], and I/β for [B], yields an equilibrium constant of the form $I/(A - I)$, where $A = \alpha\beta$. The temperature dependence of the equilibrium constant is thus given

$$\ln\left(\frac{I}{A-I}\right) = \frac{B}{T} + C, \tag{1}$$

where $\Delta H^\circ = -RB$, and $\Delta S^\circ = RC$.

Young and Westerdahl (YW) successfully used Eq. (1) to obtain a ΔH° value from Raman data for a two-state equilibrium.[33] Because β cannot be measured readily, their procedure was to choose A values until a plot of $\ln[I/(A-I)]$ yielded linearity in $1/T$. B was assumed to be constant, ie., ΔH° is constant, or ΔC_p° equals zero. YW then determined B and C from least squares using this single value of A. The method was later modified by varying A to give a minimum in the least squares standard error of fit.[12] A version of this modified procedure was employed initially in this work with the data of Table I, and it yielded A values between 26.4 and 34.0. However, this method is strongly dependent upon the scatter of data and thus a new procedure was adopted here instead.

Equation (1) is linear in terms of $\ln[I/(A-I)]$ vs $1/T$, but it is highly nonlinear in terms of I vs T or t. From the data of Table I, a plot of Eq. (1) using least squares values of A, B, and C (determined by methods described subsequently) yields a pronounced sigmoid shape in terms of I vs t, Fig. 2, solid curve. The maximum value of the absolute slope of the sigmoid curve corresponds to the inflection point, shown by the (perpendicular) bar at about 41 °C. This slope value gives rise to the new method of determining A, B, and C. The

essential feature of the method involves matching the slope at the inflection, as closely as possible, to the linear least squares slope, $-0.070\,847$, from $I = 22.636 - 0.070\,847\,t$. See the juxtaposition of the dashed (linear least squares) straight line, and the solid nearly straight segment of the sigmoid curve in Fig. 2 between about -25 and 100 °C.

Slopes of sigmoid curves corresponding to Eq. (1) plotted in terms of I vs t are given by the following equation which results from differentiation of Eq. (1) with respect to T:

$$\frac{dI}{dt} = \frac{dI}{dT} = \frac{-BI(A-I)}{AT^2}. \tag{2}$$

The maximum absolute value of dI/dt corresponds to the slope at the inflection point. Hence, in the present method, the A parameter is varied until the slope at the inflection approaches the linear I vs t least squares slope, as closely as possible. The method involves finding the exact inflection temperature, and then the corresponding value of dI/dt, from Eq. (2). The inflection temperature can be determined by solving Eq. (1) for I_{infl} and T_{infl} (the I and T values at the inflection point) simultaneously with the following equation arrived at by equating d^2I/dt^2 from Eq. (2) to zero,

$$I_{infl} = \frac{AT_{infl}}{B} + \frac{A}{2}. \tag{3}$$

Simultaneous solutions between Eqs. (1) and (3) for I_{infl} and T_{infl} are obtained by iteration. Then T_{infl} is used in Eq. (1) to determine the slope at the inflection, which is the maximum absolute slope.

From least square treatment of the Table I data, and the procedures described, a plot of the absolute value of the slope at the inflection was made vs A. A *minimum* in the absolute slope at the inflection occurred for $A = 28.15$. The calculated T_{infl} for $A = 28.15$ is 41.25 °C, and I_{infl} is 20.82 °C, see Fig. 2, bar. This slope, at 41.25 °C, is $-0.071\,915$, which only 1.5% larger than the linear I vs t least squares slope of $-0.070\,847$. This agreement represents the *best* possible agreement between the two different least squares approaches to the Table I data, because no inflection slope occurs below $-0.071\,915$ for other A values chosen. Moreover, the solid curve, and the dashed line of Fig. 2 are visually indistinguishable between about -25 and 100 °C, and the slopes of the two are visually identical in this region.

With regard to linear ($I = 22.636 - 0.070\,847\,t$) as opposed to nonlinear [$\ln(I/A - I) = B/T + C$] least squares fits fo the present data, it should be emphasized that there is little difference between the two fits for the temperature range of the measurements, Fig. 2. But, extrapolation leads to physically unrealistic results for the linear case, as opposed to the nonlinear case. For example, recent Raman studies of shock-compressed water indicate that partially covalent, charge transfer hydrogen bonding persists to 1437 °C at 257 kbar,[35] whereas the linear I vs t equation implies that such hydrogen bonding is totally absent above ~320 °C. The nonlinear equation, on the other hand, leads to the (qualitatively) reasonable value of 0.09 for the mole fraction of HB O–O pairs at 1437 °C. Similarly, the linear fit requires the amount of hydrogen bonding to increase linearly below -50 °C, whereas the nonlinear fit indicates that hydrogen bonding is essentially complete near 50 °C. In this regard, it is well known that pure water cannot be supercooled below about -40 °C.[36] This fact agrees with the nonlinear fit, but not with the linear fit, because homogeneous nucleation is almost certainly related to the absence of NHB defects; see the sharp bend in the solid curve, Fig. 2, below -40 °C. Thus, the importance of the linear fit is solely related to its use in obtaining parameters for the nonlinear YW equation.

The $\Delta H°$ for the reaction U→B obtained from $A = 28.15$ is -2.6_1 kcal/mol OHO, or -2.6 ± 0.1 kcal/mol OHO when all of the experimental uncertainties are considered. The corresponding $\Delta S°$ is -6.2_1 cal/deg mol OHO.

Values of $\Delta H°$ that are considered to be reliable and which result from spectroscopic measurements are listed in Table II. The quantitative agreement between the present $\Delta H°$ value of 2.6 ± 0.1 kcal/mol OHO corresponding to the intermolecular O–O stretching region, with $\Delta H°$ values from

TABLE II. Values of enthalpy (or energy) of hydrogen-bond rupture for water obtained from various methods.

Method	Intermolecular	Intramolecular	
	One-phonon	One-phonon	Two-phonon
Raman	2.6 ± 0.1 kcal/mol OHO	2.5 ± 0.6 ODO (37)[a] 2.3 ± 0.3 OHO (38) 2.5 ± 0.2 OTO (38)	2.5 OHO (31)
Infrared	...	2.3 ± 0.4 ODO (39)	2.5 ODO (36) 2.4 ODO (40)
Molecular Dynamics		2.5 OHO (41)	
Depolarized Light Scattering		3 OHO (42,20)	
Neutron Scattering		2.5 OHO (43)	
Ultrasonic		2.5, OHO (44)	

[a] Numbers in parentheses are references.

the one- and two-phonon OH-stretching regions clearly indicates that the same process is involved. The present ΔH^* value is tested by means of the heat capacity, and the ΔS^* value is examined in subsequent comparisons.

2. Determination of extra ΔH^* needed for complete separation of NHB O–O pairs

The extra ΔH^* required for complete separation of NHB O–O pairs resulting from O–H ··· O breakage is readily obtained from the standard enthalpy change for vaporization at 0 °C, $\Delta H_v^* = 10.767$ kcal/mol H_2O.[45] This value corresponds to 5.384 kcal/mol O–O pair, because there are two O–O pairs per H_2O molecule in a tetrahedral network. (Here no distinction need be made between HB or NHB O–O pairs.) Thus,

$$\Delta H_v^* = f_B(\Delta H_1^* + \Delta H_2^*) + (1 - f_B)\Delta H_2^*, \qquad (4)$$

where ΔH_v^* is the enthalpy of vaporization per mole O–O, ΔH_1^* is 2.6 kcal/mol O–O, and ΔH_2^* is the extra enthalpy required for the complete separation of the NHB O–O pairs per mole.

The value of f_B at 0 °C from the nonlinear least squares fit, Fig. 2, is given by $I(0\,°C)/28.15$, thus $f_B(0\,°C) = 0.842$. Accordingly, $\Delta H_2^* = 3.2$ kcal/mol O–O, and this value indicates that highly cohesive interactions are involved between the O–H and the O in these O–O pairs. Note that the total enthalpy necessary for the complete separation of the intact hydrogen bonds, i.e., to break the bonds and then to move the O–H away from the O as in the gas at 0 °C, is 5.8 kcal/mol O–O, which is close to the value usually quoted for the hydrogen bond enthalpy or energy.[46] However, in this work it is emphasized that a two-step process is involved. The first step is defined here as hydrogen bond rupture. The second process, as defined here, is not considered to involve a hydrogen bond *per se*, as seen for example from the lack of intermolecular Raman intensity. A more precise picture of the HB and NHB classes of interaction is presented subsequently.

3. Calculation of C_p^*

C_p^* for liquid water may be calculated using a relation derived by Frank.[47] According to this derivation the standard heat content of liquid water considered as an ideal solution is given by

$$H_l^* = f_B H_B^* + f_u H_u^* \qquad (5)$$

or by

$$H_l^* = H_u^* + f_B \Delta H^*, \qquad (6)$$

where $\Delta H^* = H_B^* - H_u^*$. Differentiation of Eq. (6) with respect to T yields the relation

$$C_{p_l}^* = C_{p_u}^* + f_B \Delta C_p^* + \Delta H^* \left(\frac{\partial f_B}{\partial T}\right)_p. \qquad (7)$$

From $K = f_B/(1 - f_B)$ and $(\partial \ln K/\partial T)_p = \Delta H^*/RT^2$, one obtains $(\partial f_B/\partial T)_p = f_B(1 - f_B)\Delta H^*/RT^2$. Substitution for $(\partial f_B/\partial T)_p$ in Eq. (7) leads to the result

$$C_{p_l}^* = C_{p_u}^* + f_B \Delta C_p^* + \frac{f_B(1 - f_B)}{R}\left(\frac{\Delta H^*}{T}\right)^2. \qquad (8)$$

The YW method described previously requires ΔH^* to be constant over the temperature range involved, and thus $\Delta C_p^* = 0$. Hence, the second term in Eq. (8) is made zero, for consistency. This term cannot exceed, and is thought to be smaller than, 0.465 cal/deg mol O–O, because $C_p^*(s) - C_p^*(g)$ is 0.552 cal/deg mol O–O at 0 °C, and $f_B = 0.842$. The third term of Eq. (8) is 6.09 cal/deg mol O–O, or 12.18 cal/deg mol H_2O. The standard heat capacity of the vapor at 0 °C is 7.905 cal/deg mol H_2O. Hence $C_{p_l}^*$ is 20.08 cal/deg mol H_2O or 1.11 cal/deg g H_2O.

The calculated heat capacity of 1.11 cal/deg g H_2O at 0 °C is in very satisfactory agreement with the experimental value of 1.01 cal/deg g H_2O, when it is considered that ideal solution thermodynamics was employed, and more importantly when it is realized that errors in ΔH^* are squared in Eq. (8). It should also be mentioned that the specific volume of water rises 3.6% over the temperature range of the present experiments. This means that relatively fewer H_2O molecules are excited in the path of the laser beam after expansion. However, a density correction was not made here because of the scatter of the data, and because the magnitude of this correction is about the same as the long term drift of the laser power. Nevertheless, this correction would be in the direction of lowering the ΔH^* value, which would improve the calculated $C_{p_l}^*$ value.

4. Entropies

Consider that S_l^* for liquid water is given by the ideal solution formulation

$$S_l^* = f_B S_B^* + f_u S_u^* - R(f_B \ln f_B + f_u \ln f_u), \qquad (9)$$

where the last term is the entropy of mixing. Substitution of $\Delta S^* = S_B^* - S_u^*$ in Eq. (9) yields

$$S_l^* = S_B^* + (f_B - 1)\Delta S^* - R(f_B \ln f_B + f_u \ln f_u). \qquad (10)$$

At 0 °C, $f_B = 0.842$ and $f_u = 0.158$. $\Delta S^* = -6.21$ cal/deg mol O–O. The accepted value of S_l^* at 0 °C is 15.166 cal/deg mol H_2O,[48] or 7.583 cal/deg mol O–O pair. Hence, from Eq. (10), $S_B^* = 11.47$ cal/deg mol H_2O. But the standard entropy of ice at 0 °C is 9.909 cal/deg mol H_2O. Therefore, S_B^* is larger by 1.56 cal/deg mol H_2O. This ~16% additional entropy means that the bonded component of water is more disordered than ice, and thus cannot be identical to ice.

One possible source of extra disorder of the HB component may be that some or most of the hydrogen bonds in the bonded form of water are not quite linear, i.e., a range of HB O–H ··· O angles somewhat less than 180° exists.

The standard entropy for the NHB form of liquid water is also readily calculated at 0 °C. $-\Delta S^* = S_u^* - S_B^* = 12.42_6$ cal/deg mol H_2O. $S_B^* = 11.47$ cal/deg mol H_2O. Hence $S_u^* = 23.90$ cal/deg mol H_2O. However, the spectroscopic value of S^* for the gas at 25 °C is 45.106 cal/deg mol H_2O,[48] which upon adding $C_p \ln(273.15/298.15)$ yields an S^* value of ~44.4 cal/deg mol H_2O at 0 °C. Because this value is larger than S_u^* by ~20.5 cal/deg mol H_2O, it is obvious that the NHB component is much more ordered and much more liquid-like than the gas. This order is related to the strong cohesive forces which refer to the ΔH_2^* value of

3.2 kcal/mol O–O pair, and probably arises from strong electrostatic (multipole), induction, and dispersion forces.[49]

Finally, it should be noted, that although S° (g, 273.15 K) $\gg S^*_\beta$, it is nevertheless reasonable to use the gas value for $C^*_{p_\beta}$ in Eq. (8). The heat capacity of ice at 0 °C is nearly equal to the value for the vapor at that temperature, i.e., only higher by 1.104 cal/deg mol H_2O. The dominant factor in the high heat capacity of the liquid, compared *either* to ice or to steam, is clearly the presence of the U⟶B or NHB⟶HB equilibrium and the large ΔH^*_1 associated with it.

C. Contour analysis and mode softening

Computer decompositions of the low-frequency contours were accomplished by use of an analog computer. Raman amplitudes (the difference between the total amplitude and the base line) were transferred manually to horizontal base lines using frequency increments of 12.5 cm^{-1}. Analog decomposition was then carried out using two (nominal 60 and 170 cm^{-1}) Gaussian components. It was found in all cases, however, that the component intensity below 60 cm^{-1} had to be truncated such that it not exceed the observed intensity and so that its tail not be allowed to extend (slightly) into the anti-Stokes region. The 60 cm^{-1} component that resulted was thus only Gaussian in shape above its peak, i.e., it could be considered to be skewed to high frequencies. Also neutron inelastic scattering data yield a peak in the spectral density function of water at ~100 cm^{-1} with a shoulder at 60 cm^{-1}.[50] This neutron observation might explain the nonsymmetric Raman shape seen here for the 60 cm^{-1} component. Furthermore, a nearly identical nonsymmetric Raman shape has been seen for an isolated low-frequency component of molten B_2O_3 at ~28 cm^{-1}.[28,29] With the two components described, a consistent set of component peak frequencies and full widths at half-height (FWHH) was obtained.

The component peak frequencies are plotted vs temperature in °C in Fig. 3. The FWHH values (not shown) were nearly constant, ~65 cm^{-1} for the 60 cm^{-1} component, and ~140 cm^{-1} for the 170 cm^{-1} component.

Decreases in the component frequencies are evident from Fig. 3. Least squares equations referring to these decreases are shown in the figure. The frequency change of the 170 cm^{-1} component agrees satisfactorily with recent results.[25]

The frequency decrease observed for the 170 cm^{-1} component with temperature rise is consistent with a decrease in the stretching force constant of the partially covalent H ··· O bond of the HB O–H ··· O unit. Such a decrease in the H ··· O stretching force constant is consistent with an increase in the H ··· O bond distance, as seen from the inverse relationship between bond distance and force constant.[51] However, the x-ray RDF shows little increase in the nearest-neighbor O–O distance over the small temperature range involved here.[52] Hence, an increase in the H ··· O distance would seem to demand a decrease in the O–H ··· O angle, if the O–O distance remains essentially constant.

The frequency decrease observed for the 60 cm^{-1} component also indicates that a decrease in some force constant has occurred, probably the O–H ··· O bending force constant. An *increase* in the O–H ··· O angle in the direction of 180° would thus normally be expected, because this effect would lower the O–O repulsion by moving the oxygen atoms farther apart, cf. Refs. 53, 54 for vitreous SiO_2. But an increase in the O–H ··· O angle is extremely unlikely, because more nearly linear hydrogen bonds are generally thought to be stronger, not weaker. Moreover, this explanation for the 60 cm^{-1} frequency decrease is just the opposite of that for the 170 cm^{-1} frequency decrease. Obviously, another more fundamental effect is involved.

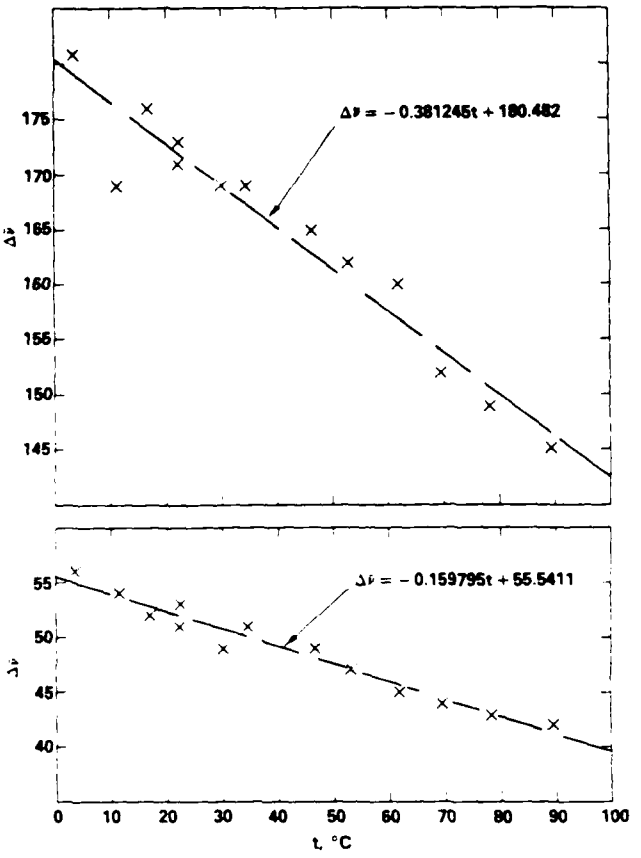

FIG. 3. Raman component frequencies (two component analysis) vs temperature in °C, from Bose–Einstein corrected spectra for water.

It is virtually certain that the occurrence of intermolecular Raman intensity for water is the result of the partial covalency of, or of the charge transfer into, the H ··· O part of the O–H ··· O units.[4,5,6] Furthermore, this partial covalency has been shown to decrease as the O–H ··· O angle decreases below 180°,[6] although a concomitant increase in the H ··· O distance would also have similar effects. At any rate, a decrease in the partial covalency of the H ··· O bond, would decrease *both* the O–H ··· O stretching and bending force constants seen here, because both the 60 and the 170 cm^{-1} components are Raman active by virtue of this partial covalency. Furthermore, when the O–H ··· O angle becomes very small, say 150° or less, and when the H ··· O distance is large, for example, ~2.4 Å, no intermolecular Raman intensity whatsoever would be expected. Sec. III D. In this case other types of cohesive interactions would be involved. Secs. III B 2, III B 4, and III D, where an NHB OH-stretching frequency near 3650 cm^{-1} results.

Three component analyses of the low-frequency contour were also carried out using the truncated or skewed 60 cm^{-1} component, plus two other completely symmetric Gaussian components.[55] The three component fits were somewhat better than those described, but they do not alter the preceding conclusions.

A consequence of the O–H ··· O bending hypothesis is that the present thermodynamic treatments must involve average $\Delta H°$ and $\Delta S°$ values, where these averages refer to the HB and NHB population groups. Nevertheless, it is evident that consistent definitions of these groups are involved, because of the quantitative agreements between $\Delta H°$ values from the intermolecular and the one- and two-phonon OH-stretching regions from both Raman and infrared measurements, as well as other nonvibrational types of measurements, Table II.

The average nature of the $\Delta H°$ and $\Delta S°$ values in terms of OH-stretching vibrations refers to the large spectral widths observed. The two population classes are evident from the loss of Raman intensity in the HB OH-stretching region and the concommitant intensity gain in the NHB OH-stretching region with temperature rise. The regions are separated by an isosbestic point which occurs when the compound frequencies, and thus, the corresponding average thermodynamic quantities, do not change rapidly with temperature. These spectroscopic features of water are all involved in the quantitative $X(Z,Z+X)Y$ OH-stretching and in the corresponding difference spectra described next.

D. Isosbestic point and Raman difference spectra from the fundamental OH-stretching region

Raman spectra obtained between 3.5 and 72.0 °C with the HG2S double monochromator under precisely constant conditions of excitation and detection are shown in Fig. 4. The laser beam position in the filled Raman cell was held exactly fixed at all temperatures by use of Newton's rings, as described in Sec. II. The spectra shown in Fig. 4 were obtained with dc detection and refer to the $X(Z,X-Z)Y$ geometry, which was used throughout this work. [Quantitative Raman spectra corresponding to the $X(Y,X+Z)Y$ $X(ZZ)Y$, and $X(ZX)Y$ geometries for water are presented in the preceding article.[56]]

The $X(Z,X+Z)Y$ spectra of Fig. 4 display a precise isosbestic point at 3425 cm^{-1}. No evidence whatsoever is present in Fig. 4, or in the large original spectral tracings that would indicate that the crossings occur within a sizable area; or, that the crossings occur at the same frequency, but not at the same intensity. [Precise isosbestic points were also observed for the $X(Y,X+Z)Y$, $X(ZZ)Y$, and $X(ZX)Y$ spectra, and a precise isosbestic point was observed for the α^2 spectrum as well, e.g., from $I(VV)-4/3I(VH)$.[56] This precise new α^2 isosbestic point indicates that the data of Ref. 32 are in error.]

The isosbestic point of Fig. 4 may be understood by the following analysis which employs HB and HHB interactions.

Consider that the Raman intensity $I(\omega,t)$, where ω refers to frequency and t to temperature, is given by

$$I(\omega,t) = I_{HB}(t) + I_{NHB}(t), \tag{11}$$

or

$$I(\omega,t) = \sum_{\omega} J_{\omega} C_{\omega}(t) + \sum_{\omega} J'_{\omega} C'_{\omega}(t), \tag{12}$$

where the index ω can run over the entire OH-stretching contour to allow for component overlap, J_ω is a constant for a particular ω and refers to HB interactions, and J'_ω is the corresponding constant, but refers to NHB interactions, and C_ω and C'_ω are temperature dependent HB and NHB concentrations, respectively. Also

$$\sum_{\omega} C_{\omega}(t) + \sum_{\omega} C'_{\omega}(t) = \alpha, \tag{13}$$

where α is a constant,[34] i.e., conservation of mass applies. At the isosbestic point, $\omega = i$, $I(\omega,t) = \text{const.}$ and $dI(\omega,t)/dt = 0$. Hence,

$$J_i \frac{dC_i(t)}{dt} + J'_i \frac{dC'_i(t)}{dt} = 0, \tag{14}$$

and

$$\frac{dC_i(t)}{dt} = -\frac{dC'_i(t)}{dt}. \tag{15}$$

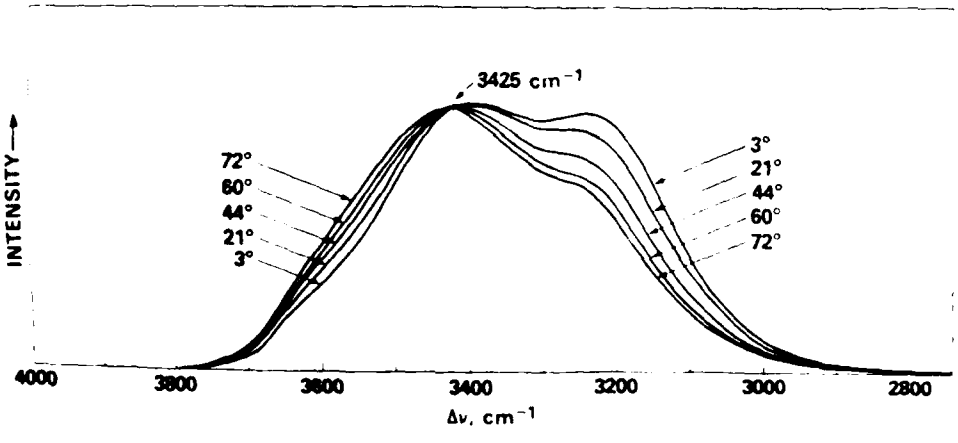

FIG. 4. Quantitative (absolute) Raman spectra in the OH-stretching region obtained under rigorously constant conditions of excitation intensity and detection geometry. Note the isosbestic point at 3425 cm^{-1}, where all spectra have the same intensity. $X(Z,Z+X)Y$.

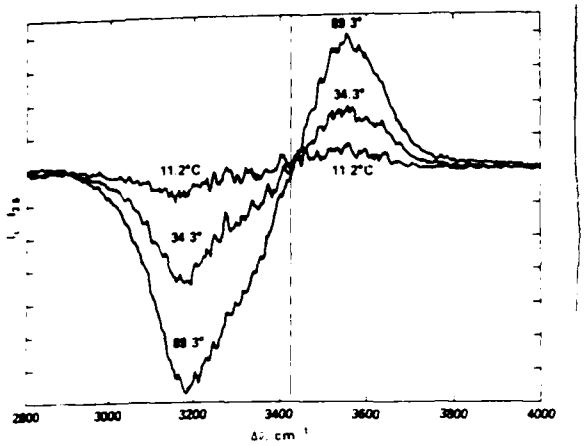

FIG. 5. Raman difference spectra from water in the fundamental (one-phonon) OH-stretching region. Note the isosbestic frequency at 3425 cm^{-1}.

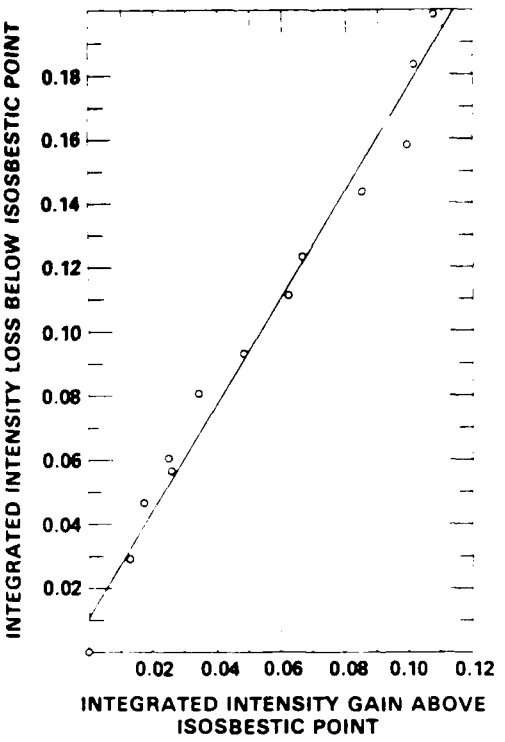

FIG. 6. Integrated Raman intensity gain above the isosbestic point vs integrated intensity loss below, see Fig. 5. $X(Z,Z+X)Y$.

Substitution of Eq. (14) into Eq. (15) yields

$$(J_i - J_i')\frac{dC_i(t)}{dt} = 0. \tag{16}$$

But, $dC_i(t)/dt$ cannot reasonably be zero.[57] Therefore, $J_i = J_i'$ at the isosbestic point. As both concentrations $C_i(t)$ and $C_i'(t)$ change with temperature, the equality of J_i and J_i' requires the Raman intensity at the isosbestic point to remain constant, because the intensity per mole liter is the same for either species or interaction. Furthermore, it should be made clear that the equality of J_i and J_i' definitely does not mean that the two species or two classes of interactions refer to the same structure. On the contrary, the interaction energy between H_2O molecules is a function of the O–O separation, of two polar angles, and three Euler angles.[58] This means that the NHB and HB classes of interaction may be regarded as separate volume elements in this 6 space. Hence, in the specific case of the isosbestic point, mapping of the 6 space into the intensity vs frequency space leads to a situation in which two different interactions, HB and NHB, have the same molar intensity, $J_\omega = J_\omega'$, at $\omega = i$.[58]

Raman difference spectra were obtained with the T800 triple monochromator for temperatures from 3.5 to 89.3 °C. (The noise levels are larger than those of Fig. 4 because the conditions were different, and amplification of the differences was also involved.) The intensity differences are all zero at 3425 cm^{-1}, as shown, for example, by spectra corresponding to three temperatures (of a total of 12) in Fig. 5. The difference spectra of Fig. 5 were obtained using digitized data and the computer described in Sec. II. From Fig. 5 it is evident that the integrated intensity loss below 3425 cm^{-1}, upon temperature rise, is accompanied by a somewhat smaller intensity gain in the integrated intensity above 3425 cm^{-1}. This observation suggests that the HB OH-stretching oscillators are replaced by NHB OH-stretching oscillators at a higher frequency. Moreover, the molar intensity from the NHB OH-stretching oscillators must be relatively smaller than those of the HB oscillators. But before it can be concluded that there is an exact conservation between oscillators of the two classes, it is necessary to examine the intensity differences quantitatively.

The NHB integrated intensity gain above 3425 cm^{-1} is plotted vs the HB integrated intensity loss below 3425 cm^{-1} (absolute values) in Fig. 6. Proportionality is definitely evident from Fig. 6 for the temperature range of 3.5 to 89.3 °C. The linear least squares fit of the data (including the point at the origin) is shown by a straight line.

The proportionality evident from Fig. 6 may be seen to arise from conservation of HB and NHB OH-stretching oscillators. Consider then the integrated Raman intensity below 3425 cm^{-1} in the OH-stretching region, $I_{HB}(t)$, is given by

$$I_{HB}(t) = \sum_\omega J_\omega C_\omega(t) = \bar{J}_{HB} \sum_\omega C_\omega(t), \tag{17}$$

where $C_\omega(t)$ is the temperature dependent concentration of OH-stretching oscillators at a single frequency ω, and $\bar{J}_{HB}$ is an average scattering per total mole of OH oscillators per liter as defined by the second equality of Eq. (17). The integrated Raman intensity above 3425 cm^{-1} in the NHB OH-stretching region, $I_{NHB}(t)$, is similarly given by

$$I_{NHB}(t) = \sum_\omega J_\omega' C_\omega'(t) = \bar{J}_{NHB} \sum_\omega C_\omega'(t). \tag{18}$$

Substitution of Eqs. (17) and (18) into Eq. (13), which involves conservation of the total HB and NHB OH-stretching oscillator concentrations, and rearrangement yields

$$-I_{HB}(t) = \left(\frac{\bar{J}_{HB}}{\bar{J}_{NHB}}\right) I_{NHB}(t) - \alpha \bar{J}_{HB}. \tag{19}$$

A difference equation results from Eq. (19) for temperatures t_2 and t_1, where $t_1 = \text{const} = (\gamma)$, thus

$$-[I_{HB}(t_2) - I_{HB}(\gamma)] = \left(\frac{\bar{J}_{HB}}{\bar{J}_{NHB}}\right)[I_{NHB}(t_2) - I_{NHB}(\gamma)]. \quad (20)$$

From Eq. (20) it is obvious that the absolute value of the integrated difference $-[I_{HB}(t_2) - I_{HB}(\gamma)]$ increases in *direct proportion* to the increase in the other integrated difference, $[I_{NHB}(t_2) - I_{NHB}(\gamma)]$, as t increases above γ.

In regard to Eq. (13) and to the $[U] + [B] = \alpha$ conservation condition in the YW derivation, it should be made clear that because the ΔH° value from the OH-stretching region agrees with the low-frequency intermolecular ΔH° value, it is apparent that the same two population classes HB and NHB, must be involved in both cases. Hence, Eq. (13) is simply a more detailed expression of $[U] + [B] = \alpha$, i.e., $\Sigma_\omega C'_\omega(t) = [U]$ and $\Sigma_\omega C_\omega(t) = [B]$. Moreover, this identity of definitions must be demanded, if exactly the same process is involved in the intermolecular and intramolecular Raman measurements. A further consequence of the formulation of Eq. (13) is that a range of structures must exist for HB and NHB population classes. However, this range of structures in no way precludes the present thermodynamic analysis, because the ΔH° and ΔS° values refer to *averages* over the configurations involved.

It should also be noted that the conclusions resulting from Figs. 4, 5, and 6, and in particular Eq. (20), provide definite evidence for the presence of the HB→NHB transformation, but they fail to provide any evidence whatsoever for Fermi resonance,[59] or for untested and contrived explanations, such as electrical anharmonicity.[60–63] Futhermore, the present data clearly eliminate assignments of the 3630 cm^{-1} shoulder in the OH-stretching region to a combination vibration.[64] On the other hand, the data of Figs. 4, 5, and 6 agree completely with molecular dynamics, cf. Fig. 11 of Ref. 65.

E. Estimation of NHB O–H O angles and distances using vibrations from vicinal surface silanol groups on vitreous silica

The Raman spectrum from dilute HDO in D_2O (1 mol H_2O in D_2O, 25 °C) displays a broad shoulder component centered ner 3628 cm^{-1} due to NHB OH stretching, in addition to the main peak at ~3435 cm^{-1} from HB OH stretching.[66] This HDO spectrum is useful in the following considerations.

Silanol groups, Si–O–H (three Si bonds not expressed), like HDO and HTO molecules,[67] involve decoupling of the stretching vibrations. The Si–O–H decoupling, however, is more complete. On a vitreous silica surface, the free (displays *P* and *R* branches[68]) OH-stretching frequency of Si–O–H is 3750 cm^{-1},[68–70] and the Si vs OH stretching frequency is 970–980 cm^{-1}.[71] However, when the surface Si–O–H coverage becomes large, a broad peak develops near ~3650 cm^{-1}, in addition to the sharp 3750 cm^{-1} peak.[68–70] This 3650 cm^{-1} peak has been shown conclusively to arise from NHB or O–H O interactions between neighboring or *vicinal* silanol groups whose Si atoms are linked by a surface Si–O–Si bridge.[68–70]

From known angles and bond distances it is possible to estimate the O–H O angle and H O distance corresponding to the 3650 cm^{-1} feature. For bulk fused silica[72] or for thin surface silica films[73] the Si–O, O–O, and Si–Si nearest-neighbor distances are 1.6, 2.6, and 3.1 Å, respectively, and the Si–O–Si bridging angle is 144°.[74,75] The tilt or dihedral angle δ between bridged SiO_4 tetrahedra is about 16°,[75] and the Si–O–H angle β is near 113° (experiment)[68] or about 109° theory,[76] i.e., both values are not far from the tetrahedral angle, 109°28′. The O–H distance is 0.96 Å.[77] From these data, the calculated O–H O angles and H O distances are, respectively, 148° and ~2.4 Å ($\beta = 113°$, $\delta = 16°$), and 153° and ~2.4 Å ($\beta = 109$, $\delta = 16°$). The calculated second-neighbor O′–O′ distance (O′–Si–O–Si–O′) is 3.2 Å, but this is actually the O–O distance of the O–H O interaction involved here.

The nearest-neighbor O–O distance for ice I_h is 2.76 Å,[78] and the H ··· O distance is thus about 1.8 Å when the O–H bond distance of 0.96 Å is employed. For comparison, the H O distance corresponding to the 3650 cm^{-1} vicinal silanol frequency is almost as large as the entire nearest-neighbor O–O distance in ice I_h, that is, the vicinal H O distance is 33% larger than the ice I_h H ··· O distance. Furthermore, the vicinal O–H O angle has changed by 30° compared to the ice I_h angle; a large decrease for H-bonded systems. Accordingly, the vicinal O–H O interaction can hardly be considered as a hydrogen bond,[79] and the 150° O–H O angle and the 2.4 Å H O distance must certainly refer to a weakened interaction, clearly falling within the present definition of nonhydrogen-bonded interactions. Such large angle and distance deviations from the ice I_h values would be expectd to decrease the partially covalent or charge transfer character of the H ··· O linkage,[4–6] and would also be expected to lower the OH-stretching intensity, and preclude significant intermolecular Raman intensity in the 170 cm^{-1} region.

With regard to relative HB and NHB OH-oscillator concentrations it should be noted that sizable Raman intensity occurs at 3650 cm^{-1} for dilute HDO in D_2O.[66] The contour height at 3650 cm^{-1} is ~1/4 the peak height at 3435 cm^{-1}.[66] Thus, from the silanol calculation one would expect that a significant fraction of the interactions in this HDO–D_2O mixture would refer to O–H O angles of 150° and H O distances of 2.4 Å. Moreover, a similar situation would be expected for liquid water, because the water spectra are not changed very greatly by coupling effects.

It should be emphasized, however, that the entire spectral region from the isosbestic frequency of 3425 cm^{-1} to the limit of about 3750–3800 cm^{-1} refers to a range of NHB O–H O angles and NHB O–O distances, of which, the calculated silanol values represent a single contribution, i.e., one complexion of the ensemble.

Finally, Narten and Levy[52] have made accurate x-ray measurements of $G(r)$ for liquid water between 4 and 200 °C. Their $G(r)$ data for 4 °C show asymmetry at ~3.2–3.3 Å above the intense nearest-neighbor O–O peak at 2.9 Å. This asymmetry contribution at 3.2–3.3 Å is consistent with the present conclusions than an O–O distance of ~3.2 Å

gives rise to a frequency just above the centroid of the NHB OH-stretching component, which is 3628 cm^{-1} for HDO. The temperature dependence of the x-ray data is also consistent with the observation that the relative NHB OH-stretching intensity from HDO increases with temperature rise,[67] i.e., that the concentrations of OH oscillators involved in long O–O distnaces, ~3.2 Å, increases with increasing temperture.

IV. SUMMARY

BF correction of low-frequency Raman spectra from water and thermodynamic analysis of the resulting integrated intensities yields a ΔH° value of 2.6 ± 0.1 kcal/mol OHO for the rupture of hydrogen bonds. This ΔH° leads to reasonable values for the heat capacity and for various entropies, and is in agreement with ΔH° values obtained from vibrational spectroscopy for the one- and two-phonon OH-stretching regions, as well as from other methods such as depolarized Rayleigh scattering or molecular dynamic
Some implications of the new result are: that the low-frequency intermolecular Raman spectrum arises predominantly from partially covalent linear and/or weakly bent O–H ··· O hydrogen bonds, HB; that the breakdown of such partially covalent interactions is responsible for the high heat capacity, compared to ice or to steam; and that this breakdown produces another class of cohesive interactions, NHB, whose further complete separation would require an additional 3.2 kcal/mol O–O pair.

Quantitative (absolute) Raman spectra obtained in the OH-stretching region yield a precise isosbestic point at 3425 cm^{-1}. Such a point is indicative of an equilibrium between the HB and NHB classes of interaction. Raman difference spectra in the OH-stretching region show a rise in the total integrated intensity above the isosbestic frequency, and a decrease below. A plot of the coresponding integrals indicates direct proportionality. This fact establishes the presence of the HB⟶NHB equilibrium, and indicates that the OH-oscillator concentration is conserved in terms of the HB and NHB classes.

V. ADDENDUM

A. Volume changes and pressure effects

The equation

$$\ln[I/(28.15 - I)] = \ln[f_B/(1 - f_B)] = 13.111\,024\,9T - 3.126\,419\,25,$$

see Fig. 2, allows values of I or f_B to be calculated. Values of f_B are useful in making rough estimates estimates of the volume change, $\Delta V = V_B - V_u$, corresponding to the transformation U⟶B.

The volume change ΔV may be approximated from the ideal solution formulation

$$V_l = f_B V_B + f_u V_u = f_B V_B + (1 - f_B) V_u, \qquad (21)$$

which in terms of the volume change ΔV is

$$V_l = f_B \Delta V + V_u. \qquad (22)$$

TABLE III. Values of the partially covalent hydrogen-bonded, O–H ··· O, mole fraction, f_B, at various temperatures for water.

t, °C	f_B
0	0.842
10	0.818
20	0.794
25	0.781
30	0.768
40	0.743
50	0.717
60	0.692
70	0.667
80	0.643
90	0.619
100	0.596

If values of f_B and V_l are known for widely spaced temperatures, simultaneous solutions of Eqs. (21) or (22) yield ΔV. For temperatures of 4 and 90 °C, which span the present low-frequency Raman data, simultaneous solution yields an average ΔV value of − 1.5 cm^3/mol OHO. Alternatively, Eq. (22) may be differentiated with respect to T or to P. Then from the forced assumption that all volumes except V_l are independent of T or of P, and from substitution of the appropriate expression for $(\partial f_B/\partial T)_P$ or $(\partial f_B/\partial P)_T$, see the derivation in Sec. III B 3, values of ΔV vs. t may be calculated from known values of $(\partial V_l/\partial T)_P$ or $(\partial V_l/\partial P)_T$. When $(\partial V_l/\partial T)_P$ is equated to $\Delta V \Delta H f_B f_u/RT^2$, the values of ΔV that result are as follows: (1) 0 °C, + 0.26 cm^3/mol OHO; (2) 20 °C, − 0.75; (3) 40 °C, − 1.4; (4) 60 °C, − 1.9; and (5) 80 °C, − 2.5. Of course, because these ΔV values change both in sign and in magnitude from 0 to 80 °C, it is evident that the assumption relative to temperature independence of ΔV, V_B, or V_u is faulty, but all of the calculated ΔV values are at least *small*. Moreover, the 0 °C result agrees with a value reported by Angell, Ref. 36. The important point here is that if ΔV is small, its magnitude is in qualitative agreement with Ref. 80, where no significant change in the NHB OD-stretching component intensity relative to the HB OD-stretching component intensity could be ascertained, within the accuracy of the computer analysis employed, to roughly 10 kbar at 32 °C.

For convenience values fo f_B in 10° increments between 0 and 100 °C are listed in Table III.

It has recently been possible to obtain Raman spectra in the fundamental OH-stretching region from strongly shocked water at pressures of 257 kbar and temperatures to 1437 °C (1710 K), where the density is 2 g cm^{-3}.[35] HB and NHB classes or interactions are both definitely indicated up to 1437 °C in agreement with the present work. However, most of the hydrogen bonds are broken at 1437 °C, and the H_2O molecules are thought to be held together by other strong forces, e.g., electrostatic (multipole), induction, and dispersion. At a density of 2 g cm^{-3}, the OH-stretching vibrations of H_2O molecules held by these strong nonhydrogen-bonded forces peak just above 3400 cm^{-1}. Such extremely low NHB frequencies probably occur because the O–H bond distance lengthens, and the stretching force con-

gives rise to a frequency just above the centroid of the NHB OH-stretching component, which is 3628 cm^{-1} for HDO. The temperature dependence of the x-ray data is also consistent with the observation that the relative NHB OH-stretching intensity from HDO increases with temperature rise,[67] i.e., that the concentrations of OH oscillators involved in long O–O distnaces, ~3.2 Å, increases with increasing temperture.

IV. SUMMARY

BF correction of low-frequency Raman spectra from water and thermodynamic analysis of the resulting integrated intensities yields a ΔH° value of 2.6 ± 0.1 kcal/mol OHO for the rupture of hydrogen bonds. This ΔH° leads to reasonable values for the heat capacity and for various entropies, and is in agreement with ΔH° values obtained from vibrational spectroscopy for the one- and two-phonon OH-stretching regions, as well as from other methods such as depolarized Rayleigh scattering or molecular dynamics. Some implications of the new result are: that the low-frequency intermolecular Raman spectrum arises predominantly from partially covalent linear and/or weakly bent O–H ··· O hydrogen bonds, HB; that the breakdown of such partially covalent interactions is responsible for the high heat capacity, compared to ice or to steam; and that this breakdown produces another class of cohesive interactions, NHB, whose further complete separation would require an additional 3.2 kcal/mol O–O pair.

Quantitative (absolute) Raman spectra obtained in the OH-stretching region yield a precise isosbestic point at 3425 cm^{-1}. Such a point is indicative of an equilibrium between the HB and NHB classes of interaction. Raman difference spectra in the OH-stretching region show a rise in the total integrated intensity above the isosbestic frequency, and a decrease below. A plot of the coresponding integrals indicates direct proportionality. This fact establishes the presence of the HB⟶NHB equilibrium, and indicates that the OH-oscillator concentration is conserved in terms of the HB and NHB classes.

V. ADDENDUM

A. Volume changes and pressure effects

The equation

$$\ln[I/(28.15 - I)] = \ln[f_B/(1 - f_B)] = 13.111\,024\,9T - 3.126\,419\,25,$$

see Fig. 2, allows values of I or f_B to be calculated. Values of f_B are useful in making rough estimates estimates of the volume change, $\Delta V = V_B - V_u$, corresponding to the transformation U⟶B.

The volume change ΔV may be approximated from the ideal solution formulation

$$V_l = f_B V_B + f_u V_u = f_B V_B + (1 - f_B) V_u, \qquad (21)$$

which in terms of the volume change ΔV is

$$V_l = f_B \Delta V + V_u. \qquad (22)$$

TABLE III. Values of the partially covalent hydrogen-bonded, O–H ··· O, mole fraction, f_B, at various temperatures for water.

t, °C	f_B
0	0.842
10	0.818
20	0.794
25	0.781
30	0.768
40	0.743
50	0.717
60	0.692
70	0.667
80	0.643
90	0.619
100	0.596

If values of f_B and V_l are known for widely spaced temperatures, simultaneous solutions of Eqs. (21) or (22) yield ΔV. For temperatures of 4 and 90 °C, which span the present low-frequency Raman data, simultaneous solution yields an average ΔV value of -1.5 cm^3/mol OHO. Alternatively, Eq. (22) may be differentiated with respect to T or to P. Then from the forced assumption that all volumes except V_l are independent of T or of P, and from substitution of the appropriate expression for $(\partial f_B/\partial T)_P$ or $(\partial f_B/\partial P)_T$, see the derivation in Sec. III B 3, values of ΔV vs. t may be calculated from known values of $(\partial V_l/\partial T)_P$ or $(\partial V_l/\partial P)_T$. When $(\partial V_l/\partial T)_P$ is equated to $\Delta V \Delta H f_B f_u/RT^2$, the values of ΔV that result are as follows: (1) 0 °C, +0.26 cm^3/mol OHO; (2) 20 °C, −0.75; (3) 40 °C, −1.4; (4) 60 °C, −1.9; and (5) 80 °C, −2.5. Of course, because these ΔV values change both in sign and in magnitude from 0 to 80 °C, it is evident that the assumption relative to temperature independence of ΔV, V_B, or V_u is faulty, but all of the calculated ΔV values are at least *small*. Moreover, the 0 °C result agrees with a value reported by Angell, Ref. 36. The important point here is that if ΔV is small, its magnitude is in qualitative agreement with Ref. 80, where no significant change in the NHB OD-stretching component intensity relative to the HB OD-stretching component intensity could be ascertained, within the accuracy of the computer analysis employed, to roughly 10 kbar at 32 °C.

For convenience values fo f_B in 10° increments between 0 and 100 °C are listed in Table III.

It has recently been possible to obtain Raman spectra in the fundamental OH-stretching region from strongly shocked water at pressures of 257 kbar and temperatures to 1437 °C (1710 K), where the density is 2 g cm^{-3}.[35] HB and NHB classes or interactions are both definitely indicated up to 1437 °C in agreement with the present work. However, most of the hydrogen bonds are broken at 1437 °C, and the H_2O molecules are thought to be held together by other strong forces, e.g., electrostatic (multipole), induction, and dispersion. At a density of 2 g cm^{-3}, the OH-stretching vibrations of H_2O molecules held by these strong nonhydrogen-bonded forces peak just above 3400 cm^{-1}. Such extremely low NHB frequencies probably occur because the O–H bond distance lengthens, and the stretching force con-

stant drops, as the O–O nearest-neighbor distances in the severely bent O–H O configurations decrease.[81]

B. Polarization measurements

The 170 cm^{-1} Raman band from water has been assigned to restricted translation of H_2O molecules along the O–H ··· O direction. The 60 cm^{-1} Raman band may arise from bending of the O–H ··· O units. For the case of linear O–H ··· O interactions, point group C_{∞} the H ··· O stretching vibration $\nu_3\Sigma^+$, should be polarized, $\rho_l < 3/4$. $\nu_2\Sigma^-$ should be depolarized, $\rho_l = 3/4$. However, the H ··· O bond is only weakly covalent, and thus only very weak polarization would be expected for $\nu_3\Sigma^+$. This weak polarization may be difficult to detect experimentally.

Measurements of the depolarization spectrum, i.e., ρ_l vs $\Delta\tilde{\nu}$ were made in this work. Broad minima were observed near $\Delta\tilde{\nu} = 125\ cm^{-1}$ and $\Delta\tilde{\nu} = 425\ cm^{-1}$ (very broad). At $125\ cm^{-1}$, $\rho_l = 0.71 \pm 0.03$ (very weakly polarized), and at $425\ cm^{-1}$, $\rho_l = 0.61 \pm 0.04$ (weakly polarized). The frequency of $425\ cm^{-1}$ corresponds to the libration of the H_2O molecule around its two-fold axis.[17] At the O–H ··· O bending frequency, $50\ cm^{-1}$ (see Fig. 3) $\rho_l = 0.74 \pm 0.01$ (depolarized). Also, a sharp minimum in ρ_l was seen at 1650 cm^{-1} which corresponds to ν_2A_1 (polarized). For ρ_l values in the OH-stretching region see Ref. 13 and especially Ref. 82.

ACKNOWLEDGMENTS

The assistance of R. G. Munro with the least squares computations is greatly appreciated. This work was supported by a contract from the Office of Naval Research.

[1]E. Segrè, Rend. Lincei **13**, 929 (1931).
[2]G. Bolla, Nuovo Cimento **9**, 290 (1932); **10**, 101 (1933); **12**, 243 (1935).
[3]G. E. Walrafen and M. R. Fisher, in *Biomembranes, A Volume of Methods of Enzymology*, edited by L. Packer (Academic, New York, 1986).
[4]H. S. Frank, Proc. R. Soc. London Ser. A **247**, 481 (1958).
[5]E. Whalley and D. D. Klug, J. Chem. Phys. **84**, 78 (1986).
[6]C. N. R. Rao, in *Water, A Comprehensive Treatise*, edited by F. Franks, (Plenum, New York, 1972), Vol. 1, Chap. 3.
[7]S. A. Rice (private communication).
[8]S. Krishnamurthy, R. Bansil, and J. Wiafe-Akenten, J. Chem. Phys. **79**, 5863 (1983).
[9]M. Magat, J. Phys. (Paris) **53**, 347 (1934), **6**, 179 (1935); Ann. Phys. (Paris) **6**, 109 (1936).
[10]R. Ananthakrishnan, Proc. Indian Acad. Sci. A **2**, 201 (1935); **3**, 291 (1936).
[11]E. F. Gross, in *Hydrogen Bonding*, edited by D. Hadzi (Pergamon, New York, 1959), pp. 203–209.
[12]G. E. Walrafen, J. Chem. Phys. **36**, 1035 (1962); **40**, 3249 (1964); **44**, 1546 (1966); **47**, 114 (1967).
[13]G. E. Walfaren, in *Hydrogen-Bonded Solvent Systems*, edited by A. K. Covington and P. Jones (Taylor and Francis, London, 1968).
[14]L. A. Blatz and P. Waldstein, J. Phys. Chem. **72**, 2614 (1968).
[15]L. A. Blatz, in *Raman Spectroscopy*, edited by H. A. Szymanski (Plenum, New York, 1970), Vol. 2, Chap. 4.
[16]J. A. Bucaro and T. A. Litovitz, J. Chem. Phys. **54**, 3846 (1971).
[17]G. E. Walrafen, in Ref. 6, Chap. 5.
[18]M. A. Gray, T. M. Loehr, and P. A. Pincus, J. Chem. Phys. **59**, 1121 (1973).
[19]G. E. Walrafen, in *Structure of Water and Aqueous Solutions*, edited by W. Luck (Verlag Chemie, Weinheim, 1974).
[20]C. J. Montrose, J. A. Bucaro, J. Marshall-Coakley, and T. A. Litovitz, J. Chem. Phys **60**, 5025 (1974).
[21]M. Moskovits and K. H. Michaelian, J. Chem. Phys. **69**, 2306 (1978).
[22]O. Faurskov-Nielsen, Chem. Phys. Lett. **60**, 515 (1979).
[23]M. A. Brooker and M. Perrot, J. Mol. Struct. **60**, 317 (1980); J. Chem. Phys. **74**, 2795 (1981).
[24]Y. Yeh, J. H. Bilgram, and W. Kanzig, J. Chem. Phys. **77**, 2317 (1982).
[25]S. Krishnamurthy, R. Bansil, and J. Wiafe-Akenten, J. Chem. Phys. **79**, 5863 (1983).
[26]D. A. Draegert *et al.*, J. Opt. Soc. Am. **56**, 64 (1966).
[27]R. Shuker and R. W. Gammon, J. Chem. Phys. **55**, 4784 (1971).
[28]G. E. Walrafen *et al.*, J. Chem. Phys. **79**, 3609 (1983).
[29]S. Guha and G. E. Walrafen, J. Chem. Phys. **80**, 3807 (1984).
[30]G. Placzek, in *Handbuch der Radiologie*, 2nd ed., edited by E. Marx (Akademische Verlagsgesellschaft M.B.H., Leipzig, 1934), Vol. VI, Part 2, pp. 209–353. See pp. 210 (second paragraph) and 277 (6b) and 278 (6c).
[31]W. B. Monosmith and G. E. Walrafen, J. Chem. Phys. **81**, 669 (1984).
[32]J. R. Scherer, M. K. Go, and S. Kint, J. Phys. Chem. **78**, 1304 (1974).
[33]T. F. Young and R. P. Westerdahl, ARL 135, Office of Aerospace Research, U. S. Air Force, 1961.
[34]α is taken as constant. However, α actually decreases slightly by about 3.6% over the present temperature range, i.e., the density decreases 3.6% with temperature rise from 3.5 to 89.3 °C.
[35]N. C. Holmes, W. J. Nellis, W. B. Graham, and G. E. Walrafen, Phys Rev. Lett. **55**, 2433 (1986).
[36]C. A. Angell, in *Water, A Comprehensive Treatise*, edited by F. Franks (Plenum, New York, 1982), Vol. 7, Chap. 1.
[37]G. E. Walrafen, J. Chem. Phys. **48**, 244 (1968).
[38]G. E. Walrafen and L. A. Blatz, J. Chem. Phys. **56**, 4216 (1972).
[39]W. A. Senior and R. E. Verrall, J. Phys. Chem. **73**, 4242 (1969).
[40]J. D. Worley and I. M. Klotz, J. Chem. Phys. **45**, 2868 (1966).
[41]F. H. Stillinger and A. Rahman, J. Chem. Phys. **57**, 1281 (1972).
[42]Reference 20 directly involves NHB species concentrations. See also F. Aliotta, G. Maisano, D. Majolino, F. Mallamace, and P. Migliardo, J. Chem. Phys. (to be published).
[43]G. J. Safford (private communication). This value involves the temperature dependence of the neutron quasi-elastic scattering.
[44]C. M. Davis and T. A. Litovitz, J. Chem. Phys. **42**, 2563 (1965).
[45]"Selected Values of Chemical Thermodynamic Properties," Sec. 2, F. D. Rossini, University Microfilms, Ann Arbor, 1967.
[46]L. Pauling, *The Nature of the Chemical Bond and the Structure of Molecules and Crystals* (Cornell University, Ithaca, 1948), p. 304.
[47]H. S. Frank (private discussion).
[48]I. M. Klotz, *Chemical Thermodynamics* (Prentice-Hall, New York, 1950).
[49]F. O. Rice and E. Teller, *The Structure of Matter* (Wiley, New York, 1949), p. 64. The dipole–dipole interaction energy for stationary H_2O dipoles (O–O separation 2.84 A, $\mu = 1.85 \times 10^{-18}$ esu) is 4.30 kcal/mol (in-line) and 2.15 kcal/mol (alongside). The smaller value has roughly the right magnitude when compared to the enthalpy of 3.2 kcal/mol required for the complete separation of NHB O–O pairs. However, for the actual NHB case, e.g., for an O–O separation of 3.2 A and an O H O angle of 150°, the value is about 1 kcal/mol. Additional interactions, electrostatic (*dipole–quadrupole, quadrupole–quadrupole, etc.*), induction, and dispersion, must be involved to give a total of 3.2 kcal/mol, but this calculation is, at best, very approximate.
[50]D. J. Page, in Ref. 6, Chap. 9.
[51]R. M. Badger J. Chem. Phys. **2**, 128 (1934); **3**, 710 (1935).
[52]A. H. Narten and H. Levy, in Ref. 6, Chap. 8.
[53]M. S. Hokmabadi and G. E. Walrafen, J. Chem. Phys. **78**, 5273 (1983).
[54]G. E. Walrafen and M. S. Hokmabadi, in *Structure and Bonding in Non-Crystalline Solids*, edited by G. E. Walrafen and A. G. Revesz (Plenum, New York, 1986).
[55]Least squares equations for component frequencies $\Delta\tilde{\nu}$ vs temperature t in °C are: (1) $\Delta\tilde{\nu} = -0.103\,589t + 55.0894$, (2) $\Delta\tilde{\nu} = -0.394\,706t + 168.354$, and (3) $\Delta\tilde{\nu} = -0.262\,343t + 229.119$.
[56]G. E. Walrafen, M. S. Hokmabadi, and W.-H. Yang, J. Chem. Phys. **85**, xxxx (1986).
[57]IF $dC_i(t)/dt$ were constant, equilibria between species would be precluded, e.g., the transformation HB⇌NHB.
[58]F. H. Stillinger (private discussion).
[59]One of the first workers to propose Fermi resonance between ν_1 and $2\nu_2$ for H_2O was G. B. B. Sutherland, Proc. R. Soc. London Ser. A **141**, 535 (1933), see p. 545.
[60]H. R. Wyss and M. Falk, Can. J. Chem. **48**, 607 (1970).
[61]Y. Y. Efimov and Y. I. Naberukhin, Mol. Phys. **36**, 973 (1978).

[62]J. R. Scherer, *Advances in Infrared and Raman Spectroscopy* (Heyden, New York, 1978), Vol. 5, Chap. 3.
[63]S. Bratos and H. Ratajczak, J. Chem. Phys. **76**, 77 (1982).
[64]B. Curnutte and J. Bandekar, J. Mol. Spectrosc. **41**, 500 (1972). These workers assigned shoulders at frequencies above the ν_1 and ν_3 peaks of *HDO to combinations*, namely, $\nu_1 + \nu_T$ and $\nu_3 + \nu_T$, where ν_T is the present 170 cm^{-1} Raman band. However, the shoulder intensities increase with temperature rise, as the peak intensities decrease (Ref. 38). The intensity of ν_T, however, is shown here to *decrease* with increasing temperature. Moreover, the shoulder intensity for ν_3 of HDO continues to rise relative to the peak component to 400 °C, where the former shoulder becomes the peak (Ref. 17). Hence, the combination assignment of Bandekar and Curnutte can only be regarded as erroneous.
[65]F. H. Stillinger and A. Rahman, J. Chem. Phys. **60**, 1545 (1974).
[66]G. E. Walrafen, J. Chem. Phys. **50**, 560 (1969).
[67]G. E. Walrafen and L. A. Blatz, J. Chem. Phys. **59**, 2646 (1973).
[68]J. B. Peri, J. Phys. Chem. **70**, 2937 (1966); W. J. Mortier, J. Sauer, J. A. Lercher, and H. Noller, *ibid.* **88**, 905 (1984).
[69]D. L. Eaton, in *Silylated Surfaces*, edited by D. E. Leyden and W. T. Collins (Gordon and Breach, New York, 1980), pp. 213, 214.
[70]M. L. Hair, in *Vibrational Spectroscopies for Adsorbed Species*, ACS Ser. 137, edited by A. T. Bell and M. L. Hair (American Chemical Society, Washington, D.C., 1980).
[71]G. E. Walrafen, M. S. Hokmabadi, and N. C. Holmes, J. Chem. Phys. (to be published).
[72]N. Nagasima, J. Appl. Phys. **43**, 3378 (1972).
[73]A. H. Narten, J. Chem. Phys. **56**, 1905 (1972).
[74]R. L. Mossi and B. E. Warren, J. Appl. Crystallogr. **2**, 164 (1969).
[75]J. D. Jorgensen, J. Appl. Phys. **49**, 5473 (1978).
[76]J. Sauer and K.-P. Schroder, Z. Phys. Chem. (Leipzig) **266**, 379 (1985).
[77]G. E. Walrafen, M. Abebe, F. A. Mauer, S. Block, G. J. Piermarini, and R. G. Munro, J. Chem. Phys. **77**, 2166 (1982).
[78]S. W. Petersen and H. A. Levy, Acta Crystallogr. **10**, 70 (1957).
[79]See Fig. 2(b), p. 281 of Ref. 76, where the H_1–O_2 distance is ~2.5 Å. Also see first sentence, last paragraph, Sec. 3.2, p. 382, Ref. 76, where the 2.5 Å distance is described as referring to a "debatable" hydrogen bond.
[80]G. E. Walrafen, J. Solution Chem. **2**, 159 (1973).
[81]From the data of Ref. 35 it seems virtually certain that the trends towards a *symmetric hydrogen* bond, O–H–O, which is known to occur for the linear case when the O–O *distance approaches* about 2.4 Å, also exists for nonlinear O H O configurations as pressure decreases the O–O distance.
[82]W. F. Murphy and H. J. Bernstein, J. Phys. Chem. **76**, 1147 (1972).

DL/1113/86/2

TECHNICAL REPORT DISTRIBUTION LIST, GEN

	No. Copies
Office of Naval Research Attn: Code 1113 800 N. Quincy Street Arlington, Virginia 22217-5000	2
Dr. Bernard Douda Naval Weapons Support Center Code 50C Crane, Indiana 47522-5050	1
Naval Civil Engineering Laboratory Attn: Dr. R. W. Drisko, Code L52 Port Hueneme, California 93401	1
Defense Technical Information Center Building 5, Cameron Station Alexandria, Virginia 22314	12 high quality
DTNSRDC Attn: Dr. H. Singerman Applied Chemistry Division Annapolis, Maryland 21401	1
Dr. William Tolles Superintendent Chemistry Division, Code 6100 Naval Research Laboratory Washington, D.C. 20375-5000	1
Dr. David Young Code 334 NORDA NSTL, Mississippi 39529	1
Naval Weapons Center Attn: Dr. Ron Atkins Chemistry Division China Lake, California 93555	1
Scientific Advisor Commandant of the Marine Corps Code RD-1 Washington, D.C. 20380	1
U.S. Army Research Office Attn: CRD-AA-IP P.O. Box 12211 Research Triangle Park, NC 27709	1
Mr. John Boyle Materials Branch Naval Ship Engineering Center Philadelphia, Pennsylvania 19112	1
Naval Ocean Systems Center Attn: Dr. S. Yamamoto Marine Sciences Division San Diego, California 91232	1

TECHNICAL REPORT DISTRIBUTION LIST, 051A

Dr. M. A. El-Sayed
Department of Chemistry
University of California
Los Angeles, California 90024

Dr. E. R. Bernstein
Department of Chemistry
Colorado State University
Fort Collins, Colorado 80521

Dr. J. R. MacDonald
Chemistry Division
Naval Research Laboratory
Code 6110
Washington, D.C. 20375-5000

Dr. G. B. Schuster
Chemistry Department
University of Illinois
Urbana, Illinois 61801

Dr. J.B. Halpern
Department of Chemistry
Howard University
Washington, D.C. 20059

Dr. M. S. Wrighton
Department of Chemistry
Massachusetts Institute of Technology
Cambridge, Massachusetts 02139

Dr. A. Paul Schaap
Department of Chemistry
Wayne State University
Detroit, Michigan 49207

Dr. W.E. Moerner
I.B.M. Corporation
Almaden Research Center
650 Harry Rd.
San Jose, California 95120-6099

Dr. A.B.P. Lever
Department of Chemistry
York University
Downsview, Ontario
CANADA M3J1P3

Dr. John Cooper
Code 6173
Naval Research Laboratory
Washington, D.C. 20375-5000

Dr. George E. Walrafen
Department of Chemistry
Howard University
Washington, D.C. 20059

Dr. Joe Brandelik
AFWAL/AADO-1
Wright Patterson AFB
Fairborn, Ohio 45433

Dr. Carmen Ortiz
Consejo Superior de
Investigaciones Cientificas
Serrano 121
Madrid 6, SPAIN

Dr. John J. Wright
Physics Department
University of New Hampshire
Durham, New Hampshire 03824

Dr. Kent R. Wilson
Chemistry Department
University of California
La Jolla, California 92093

Dr. G. A. Crosby
Chemistry Department
Washington State University
Pullman, Washington 99164

Dr. Theodore Pavlopoulos
NOSC
Code 521
San Diego, California 91232

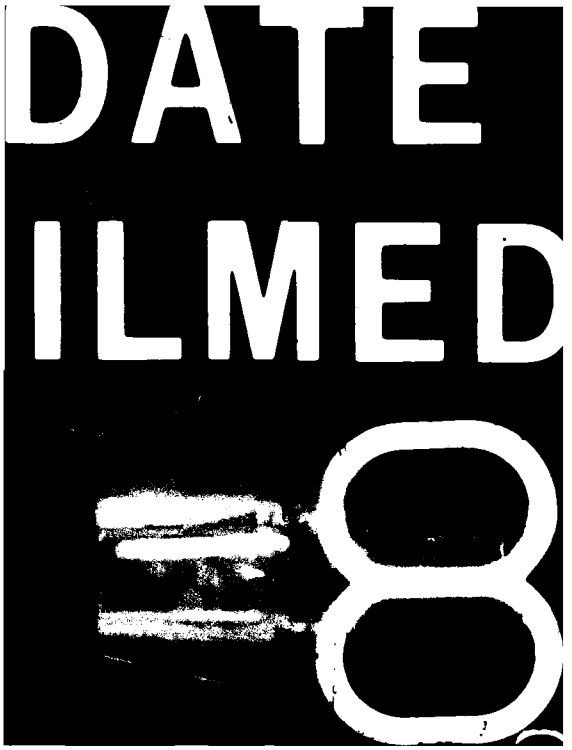
DATE
ILMED
8